Electronic Supplementary Information

A novel sodium-ion supercabattery based on vacancy defective Ni-Co-Mn ternary perovskite fluorides electrode materials

Tong Yan,[a] Rui Ding,*[a] Yongfa Huang,[a] Danfeng Ying,[a] Caini Tan,[a] Yuxi Huang,[a] Feng Yang,[a] Xiujuan Sun,[a] Ping Gao[a] and Enhui Liu [a]

[a]Key Laboratory of Environmentally Friendly Chemistry and Applications of Ministry of Education, College of Chemistry, Xiangtan University, Xiangtan, Hunan 411105, P.R. China

*E-mails: drm8122@163.com; drm8122@xtu.edu.cn

Table of contents

Experimental

Synthesis of materials

The chemicals and reagents used in this study are all of the analytical/guaranteed reagents (AR/GR) and were used without further treatment (**Table S8**). A facile one-pot solvothermal method was applied to synthesize these samples. The synthetic procedure of KMF(244)/rGO (M=Ni, Co, Mn) sample is taken out as an example since the synthetic steps of eight other KMF/rGO samples are all the same except for the usage amounts of nickel, cobalt, and manganese salts, more details of the usage amounts of reagents can be seen in **Table S9**. Firstly, 60 mg graphene oxides (GO) were dispersed in 32 mL solvents of ethylene glycol (EG) with the ultrasonic treatment for 1 h, and then 0.4 mmol $NiCl_2·6H_2O$, 0.8 mmol $CoCl_2·6H_2O$, 0.8 mmol $MnCl_2·4H_2O$, 5 mmol $KF·2H_2O$, and 0.2 g PVP-K30 were further dissolved into the solvents; Secondly, the mixture was magnetically stirred and dispersed thoroughly in an ultrasonic bath at 100 W for 30 min; Thirdly, the mixture was transferred into a 50 mL Teflon-lined stainless steel autoclave, which was heated at 180 °C for 12 h in an electric oven, and then cooled down to room temperature; Next, the yielded precipitates were centrifuged and washed with absolute alcohol for several times; Finally, the precipitates were dried at 90 °C for 12 h to obtain the final product. The synthetic of rGO is the same as the KMF(244)/rGO (M=Ni, Co, Mn) sample except for without adding nickel, cobalt, and manganese salts.

Characterizations

The phases and crystallinity properties are determined by X-ray diffraction (XRD). The surface chemical compositions and electronic structures are checked by X-ray photoelectron spectra (XPS). The morphology and size of particles are analyzed by scanning electron microscopy (SEM) and transmission electron microscopy (TEM). The crystalline microstructures are resolved by the high-resolution TEM (HRTEM) and selected area electron diffraction (SAED). The element composition and distribution are measured by inductively coupled plasma-optical emission spectrometer (ICP-OES), X-ray energy dispersive spectra (EDS), and mapping. The specific surface area, pore volume, and size distribution are examined by nitrogen isothermal sorption with Brunauer-Emmett-Teller (BET) and Barrett-Joyner-Halenda (BJH) methods. The content of reduced graphene oxide is analyzed by Thermogravimetric analysis (TGA) and differential Thermogravimetric analysis (DTG).

Electrochemical measurements

The following is the procedure of preparing electrodes: i) Mixing 70 wt.% active materials (as-synthesized KMF/rGO (811-118), rGO or commercial AC, NVPOF, and AC/NVPOF (m_{AC}:m_{NVPOF}=1:1)), 20 wt.% conductive agent of superconductive carbon black and 10 wt.% binders of polyvinylidene fluoride (PVDF) evenly with N-methyl-2-pyrrolidone (NMP)); ii) Casting the mixture onto the current collectors, where Cu foil and carbon-coated Al foil were used for anodes and cathodes respectively; iii) Drying them in a vacuum oven at 110 ℃ for 12 h; iv) Cutting them into disks with a diameter of 12 mm with the active materials mass loading of about 1.0-3.0 mg cm^{-2}. In the current work, half-cells were fabricated using the CR-2032 coin cells with active materials as working electrode (WE), a Na plate as both counter and reference electrodes (CE/RE), glass fiber (GF) as the separator, and 0.85 M

$NaPF_6$ dissolved in the mixed solvents of ethylene carbonate (EC), dimethyl carbonate (DEC) and ethyl methyl carbonate (EMC) (1:1:1 in volume) with 5% fluoroethylene carbonate (FEC) additives (MJS) as the electrolytes. Tests for the different energy storage devices (SICs, SIBs, and SICBs) were conducted via full-cells with certain mass ratios of active materials of anode and cathode (**Table S5**). All cell assemblies were performed in a highly pure Ar-filled dry glovebox (MIKROUNA, O_2 and H_2O<0.1 ppm), and all tests were carried out at room temperature (about 25 ℃) (The more detailed information of the above-mentioned materials, chemicals and reagents can be seen in **Table S8**). The test procedure of KMF/rGO (811-118) anode: we used the same cell to test the specific capacity (rate performance) at 0.02-2-0.02 A g^{-1} and cycle performance at 0.5 A g-1 for 500 cycles (before testing the cycle performance the cell was laid aside for 3 hours) of KMF/rGO (811-118) anode materials. The test procedure of NVPOF, AC and AC/NVPOF cathode half cell and SICs, SIBs and SICBs full cell: firstly, we use one fresh cell to test rate performance, and then we use another fresh cell to test cycle performance. The charge-balance ($Q_+=Q_-$) as shown in equation **(1)** was used to calculate the mass ratios of active materials of cathode and anode. The specific capacity (C_m, mAh g^{-1}), energy density ($E_{m,1}$, Wh kg^{-1}) for SICs, energy density ($E_{m,2}$, Wh kg^{-1}) for SIBs and SICBs, and power density (P_m, kW kg^{-1}) of different energy storage devices were calculated according to the equations **(2)-(5)**.

$$m_+/m_-=Q_{m-}/Q_{m+} \quad \textbf{(1)}$$

$$C_m=Q_m/3.6=It/3.6m \quad \textbf{(2)}$$

$$E_{m,1}=(C_m\Delta V)/2 \quad \textbf{(3)}$$

$$E_{m,2}=\int_0^{C_m} V dC_m \quad \textbf{(4)}$$

$$P_m=3.6E_m/t_d \quad \textbf{(5)}$$

Where m, Q_m, V, I, and t_d refer to the mass of active materials (g, for half cells, it means the mass of active materials of anode or cathode; for full-cells, it means the total masses of active materials of anode and cathode), specific charge or discharge quantity (C g^{-1}, for the anode, it means the charge quantity; for cathode and full-cells, it refers to the discharge quantity), voltage window (V), current (A) and discharging time (s), respectively.

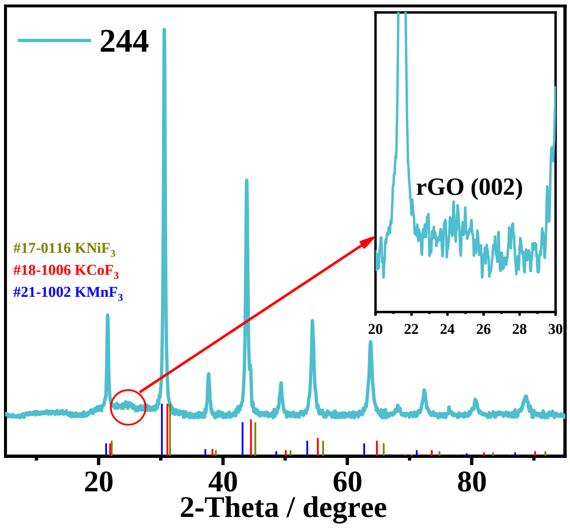

Fig. S1 XRD pattern of KMF(244)/rGO sample.

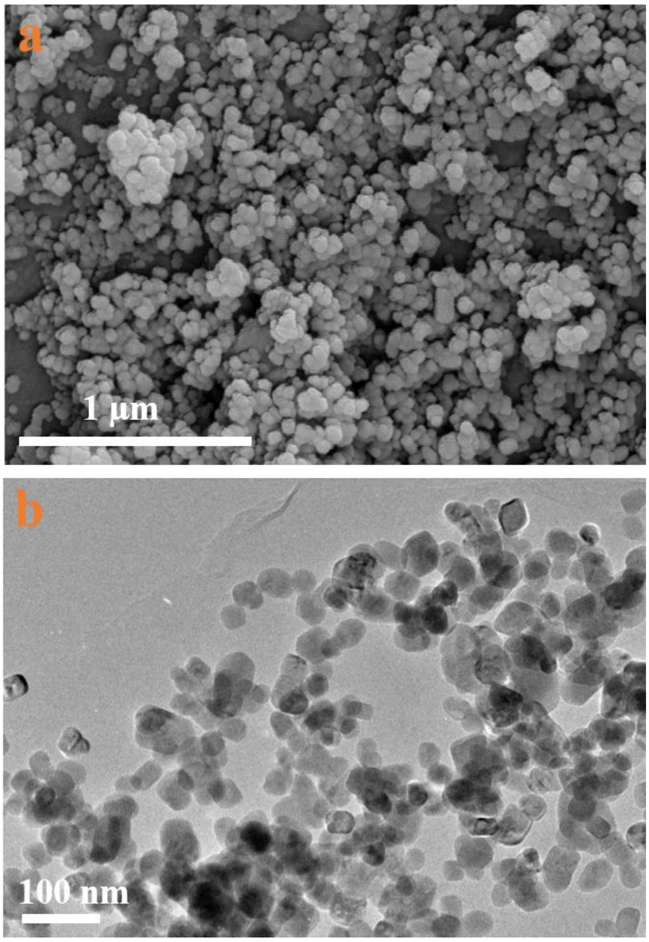

Fig. S2 SEM (a) and TEM (b) of KMF(244)/rGO samples.

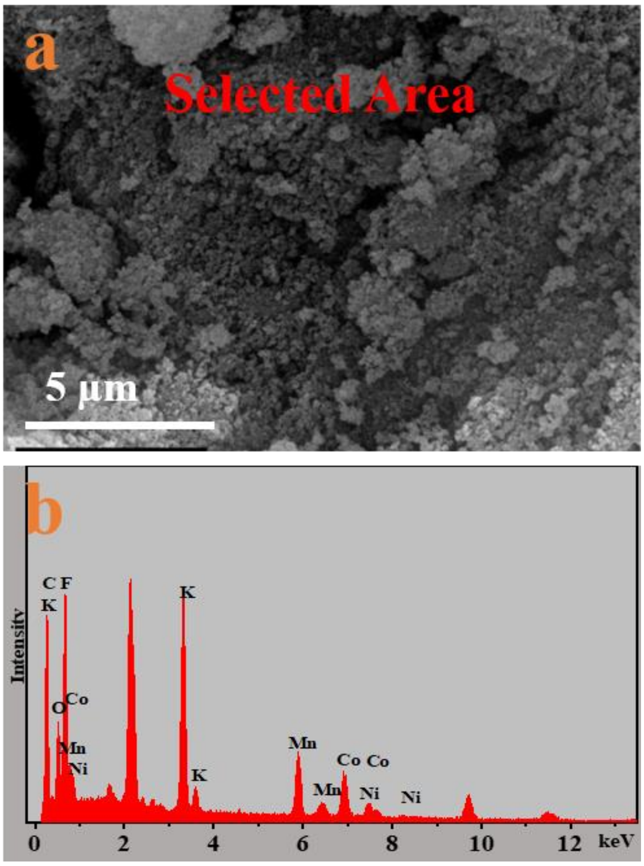

Fig. S3 SEM selected area (a) and EDS (b) of KMF(244)/rGO samples.

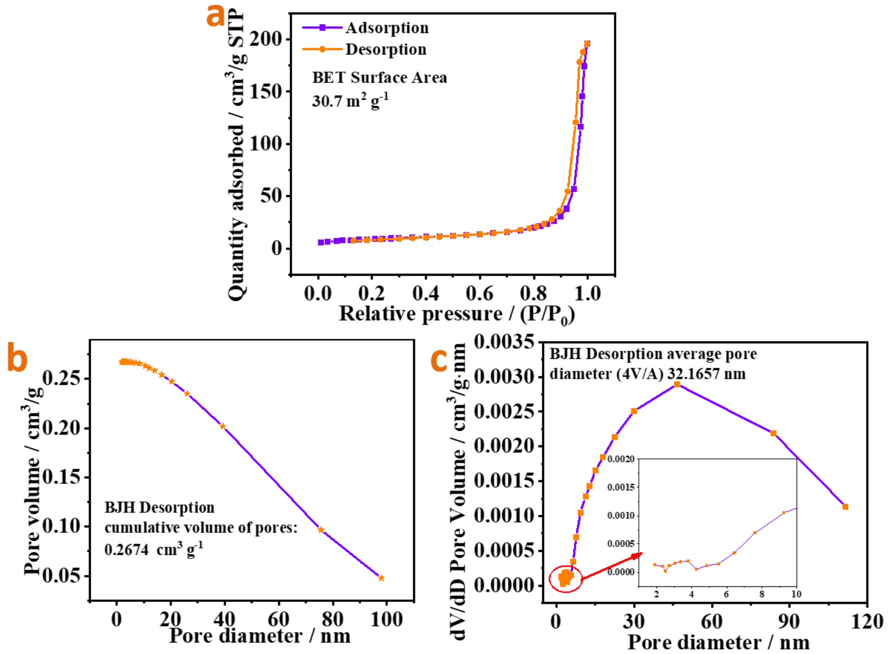

Fig. S4 N_2 sorption isotherms (a), pore volumes (b), and pore size distributions (c) of KMF(244)/rGO samples.

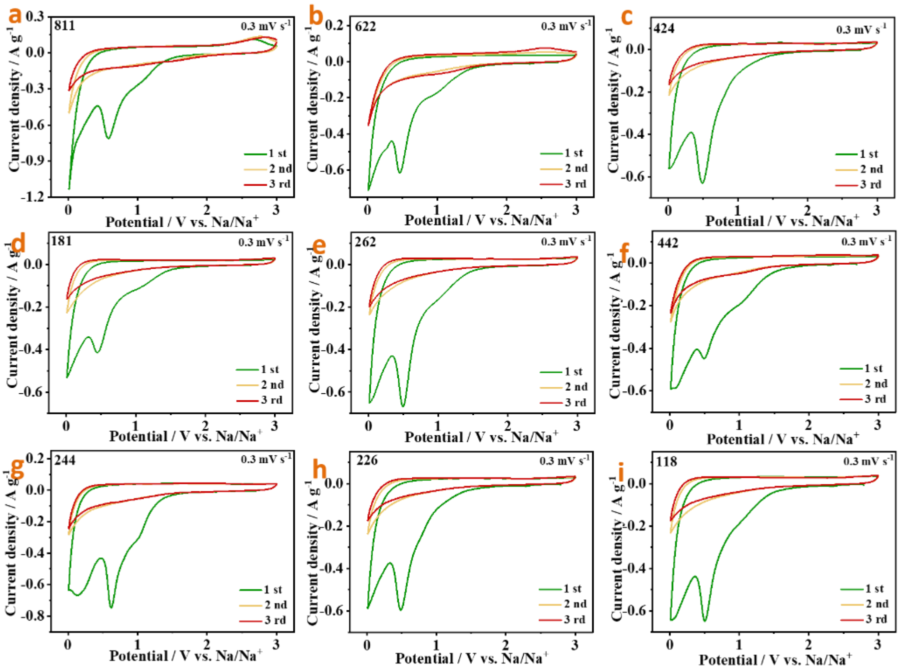

Fig. S5 CV plots for the first three cycles at 0.3 mV s^{-1} of KMF/rGO (811-118) electrodes.

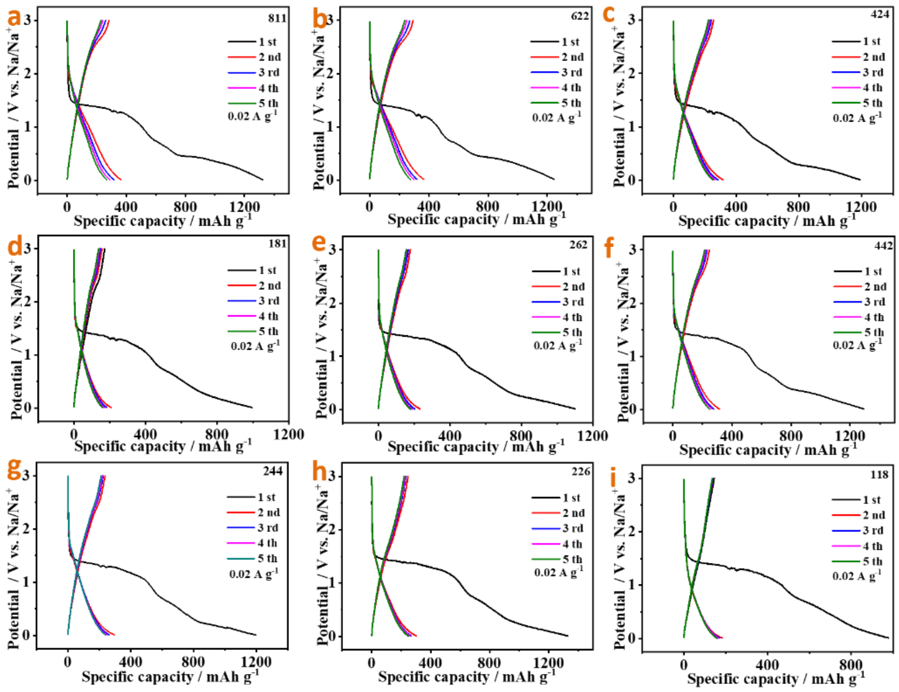

Fig. S6 GCD curves for the first five cycles at 0.02 A g^{-1} of KMF/rGO (811-118) electrode.

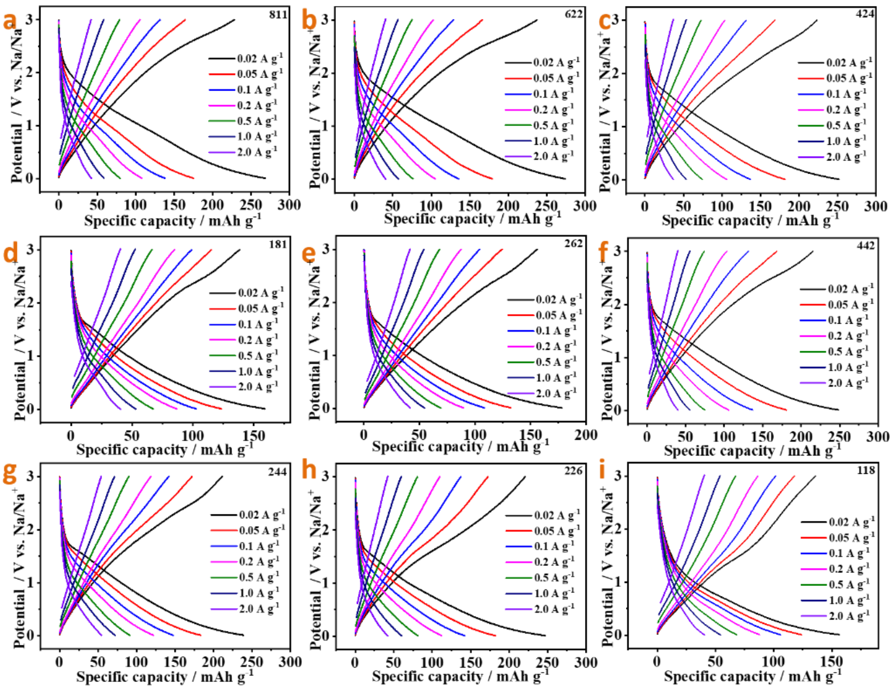

Fig. S7 GCD curves at 0.02-2.0 A g^{-1} of KMF/rGO (811-118) electrode.

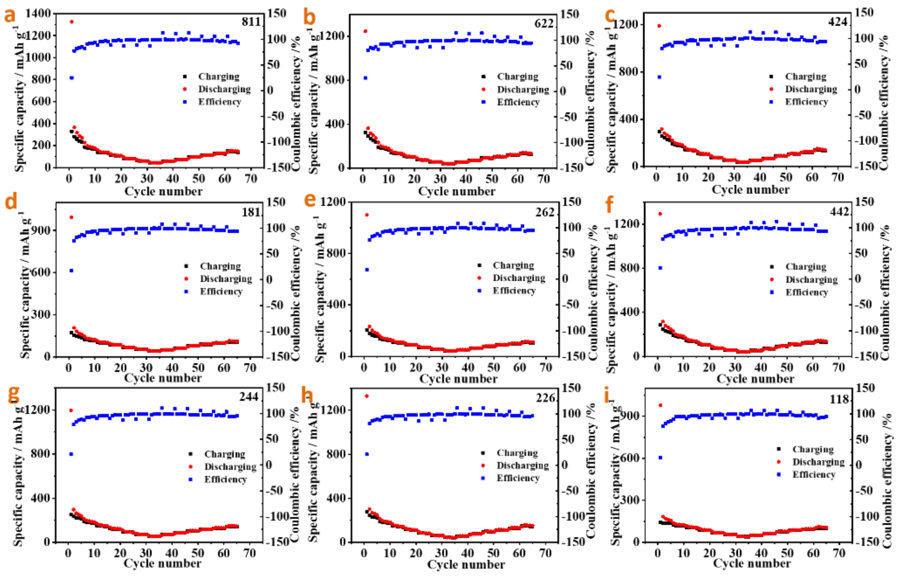

Fig. S8 Rate capability and coulombic efficiency at 0.02-2.0 A g^{-1} of KMF/rGO (811-118) electrodes.

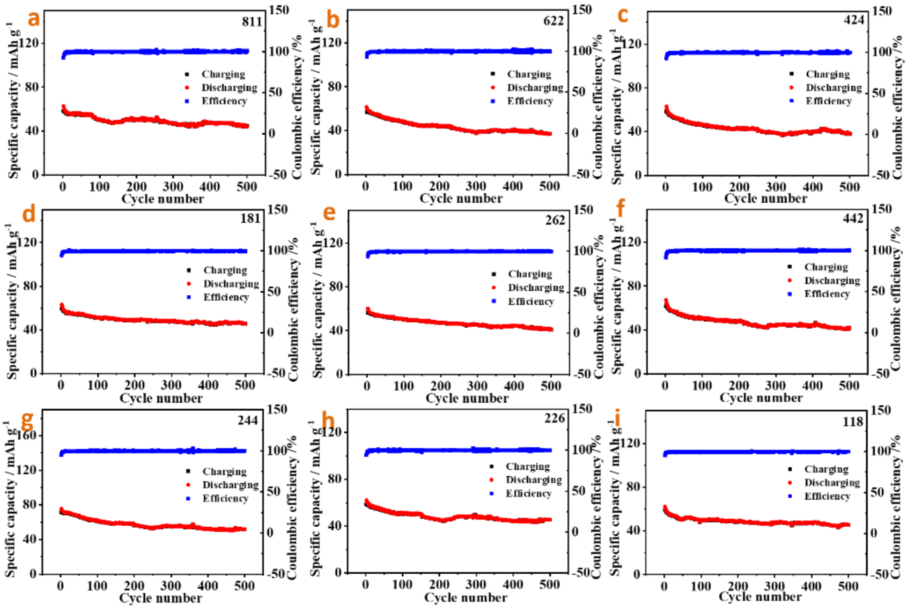

Fig. S9 Cycling behavior at 0.5 A g^{-1} of KMF/rGO (811-118) electrodes.

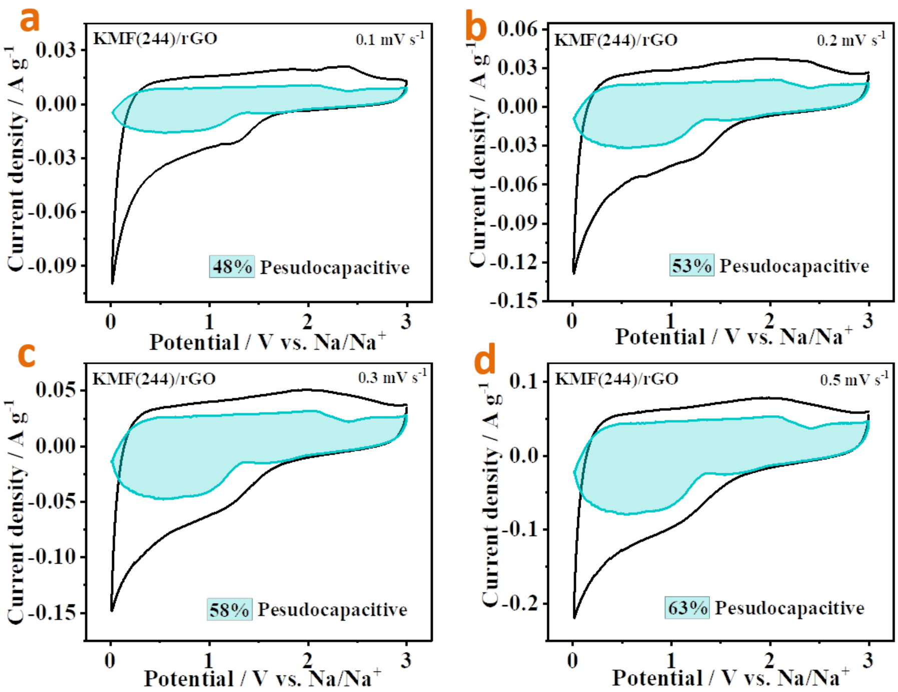

Fig. S10 Pseudocapacitive and diffusion-controlled contributions to charge storage in the KMF(244)/rGO electrode (the shaded region is the identified pseudocapacitive contribution).

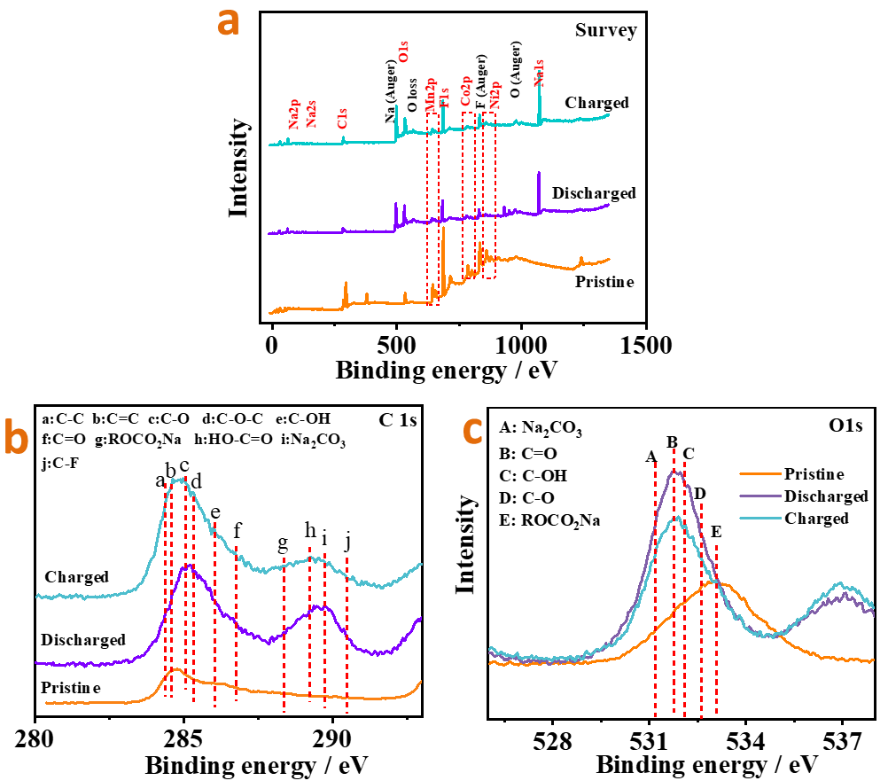

Fig. S11 Ex-situ XPS for survey scans (a), C1s (b), and O1s (c) in pristine and fully discharged/charged states of the KMF(244)/rGO electrode.

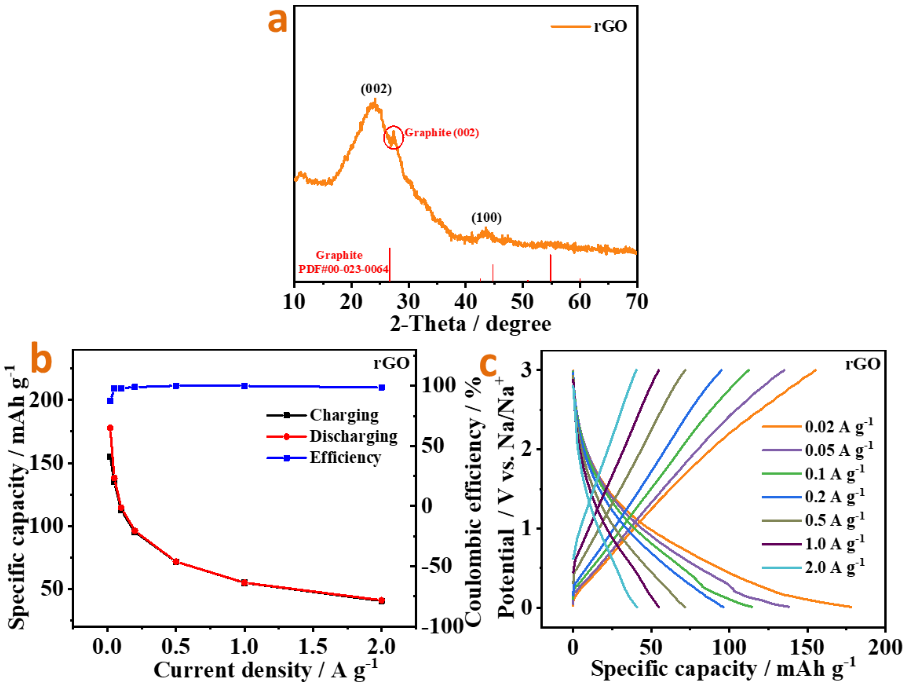

Fig. S12 XRD pattern (a), Specific capacity (b) and GCD curves (c) of rGO.

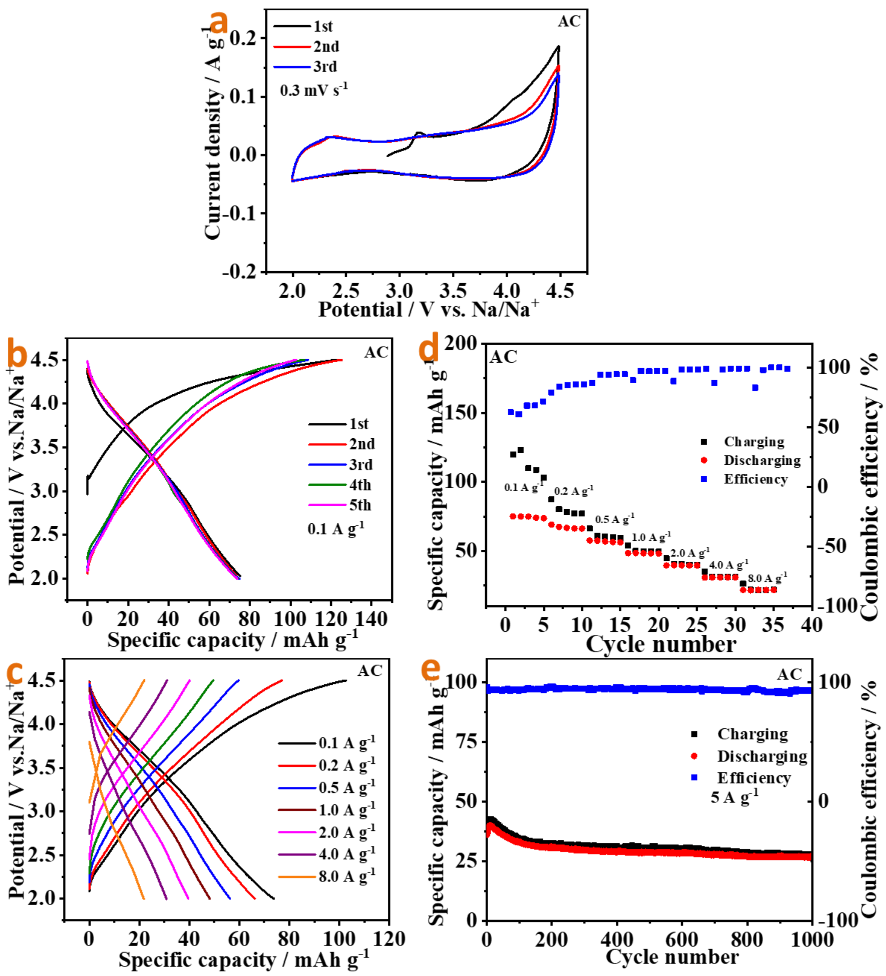

Fig. S13 Electrochemical performance of the AC electrode: CV plots for the first three cycles at 0.3 mV s^{-1} (a); GCD curves at 0.1 A g^{-1} (b); GCD curves at 0.1-8.0 A g^{-1} (c); rate performance at 0.1-8.0 A g^{-1} (d); cycling behavior at 5 A g^{-1} (e).

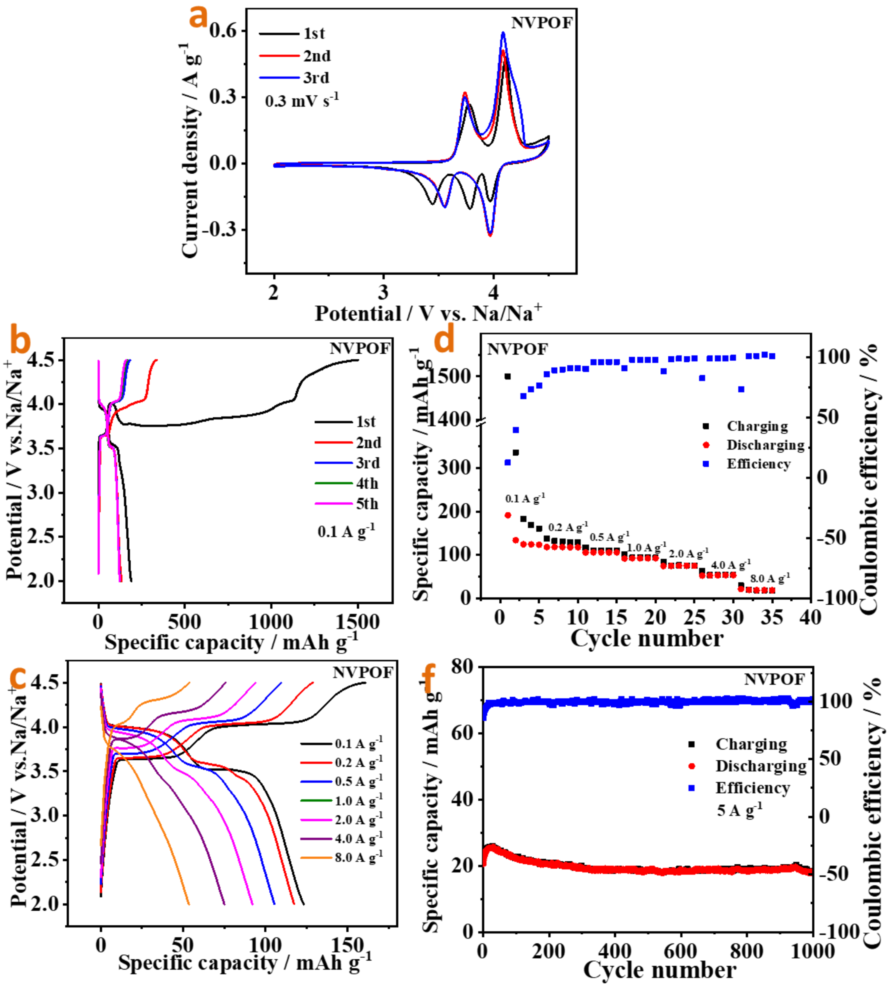

Fig. S14 Electrochemical performance of the NVPOF electrode: CV plots for the first three cycles at 0.3 mV s^{-1} (a); GCD curves at 0.1 A g^{-1} (b); GCD curves at 0.1-8.0 A g^{-1} (c); rate performance at 0.1-8.0 A g^{-1} (d); cycling behavior at 5 A g^{-1} (e).

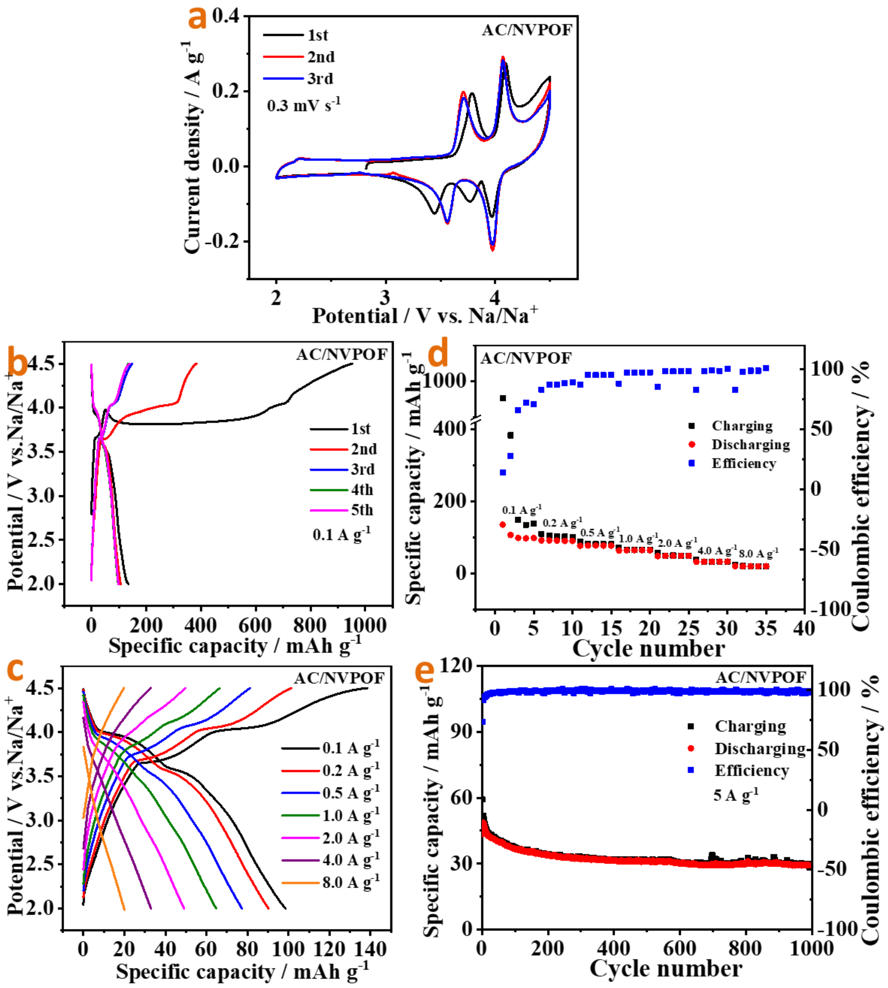

Fig. S15 Electrochemical performance of the AC/NVPOF electrode: CV plots for the first three cycles at 0.3 mV s^{-1} (a); GCD curves at 0.1 A g^{-1} (b); GCD curves at 0.1-8.0 A g^{-1} (c); rate performance at 0.1-8.0 A g^{-1} (d); cycling behavior at 5 A g^{-1} (e).

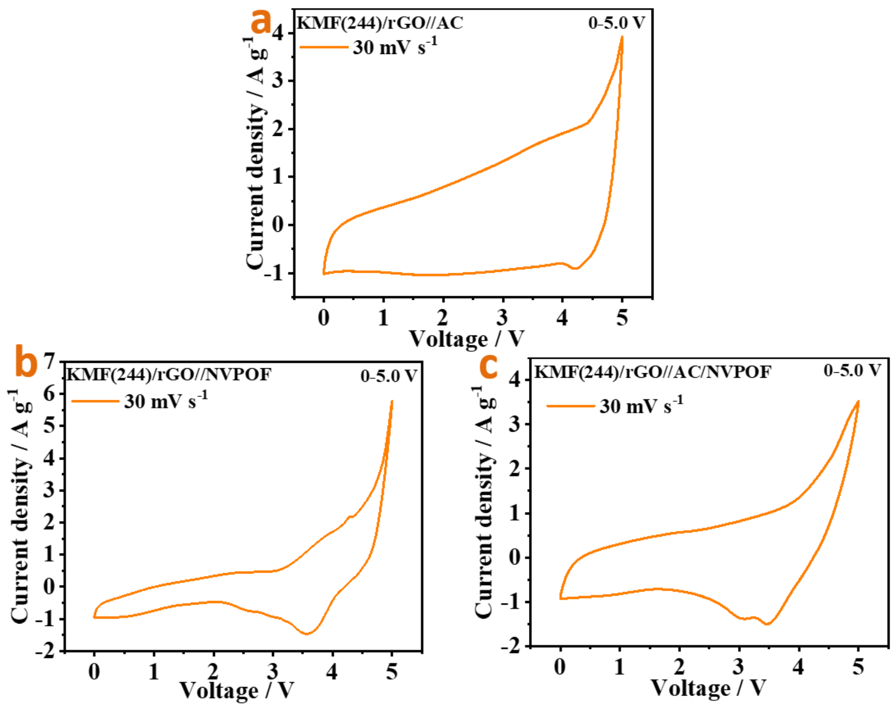

Fig. S16 Voltage windows of KMF(244)/rGO//AC SICs (a), KMF(244)/rGO//NVPOF SIBs (b), and KMF(244)/rGO//AC/NVPOF SICBs (c).

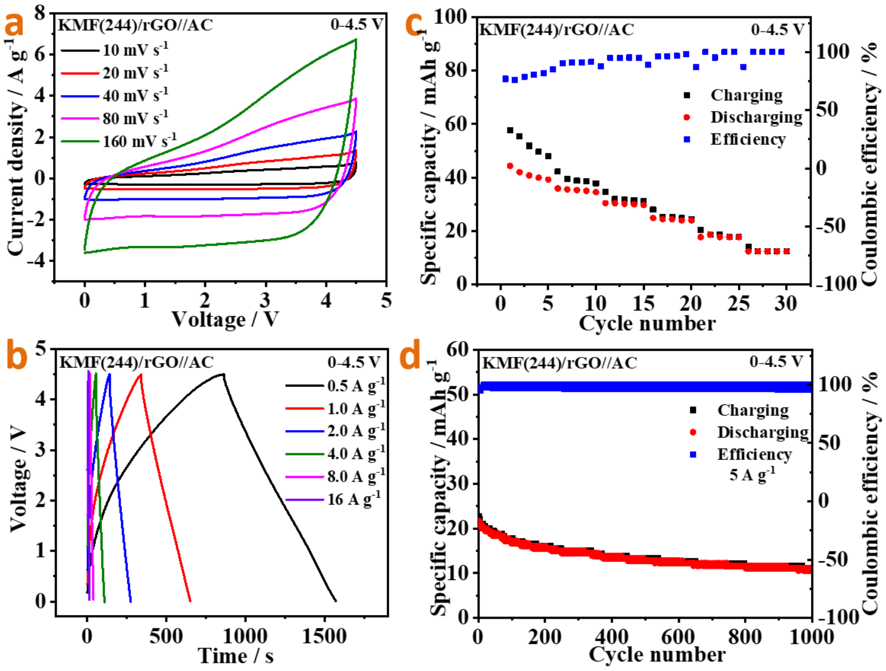

Fig. S17 CV plots at 10-160 mV s^{-1} (a), GCD curves at 0.5-16 A g^{-1} (b), rate capability at 0.5-16 A g^{-1} (c), and cycling behavior at 5 A g^{-1} (d) of the KMF(244)/rGO//AC SICs under 0-4.5 V.

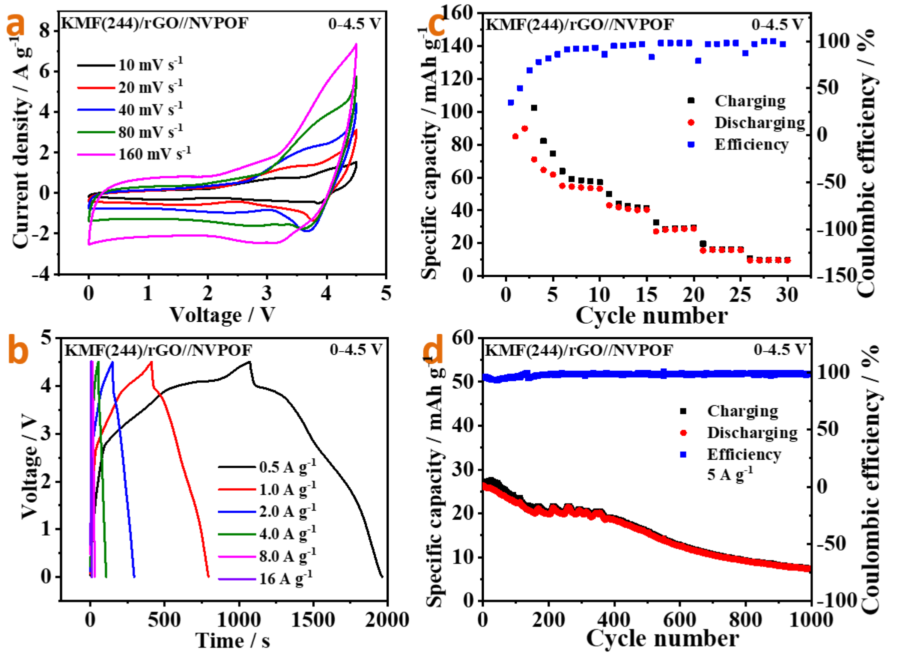

Fig. S18 CV plots at 10-160 mV s^{-1} (a), GCD curves at 0.5-16 A g^{-1} (b), rate capability at 0.5-16 A g^{-1} (c), and cycling behavior at 5 A g^{-1} (d) of the KMF(244)/rGO//NVPOF SIBs under 0-4.5 V.

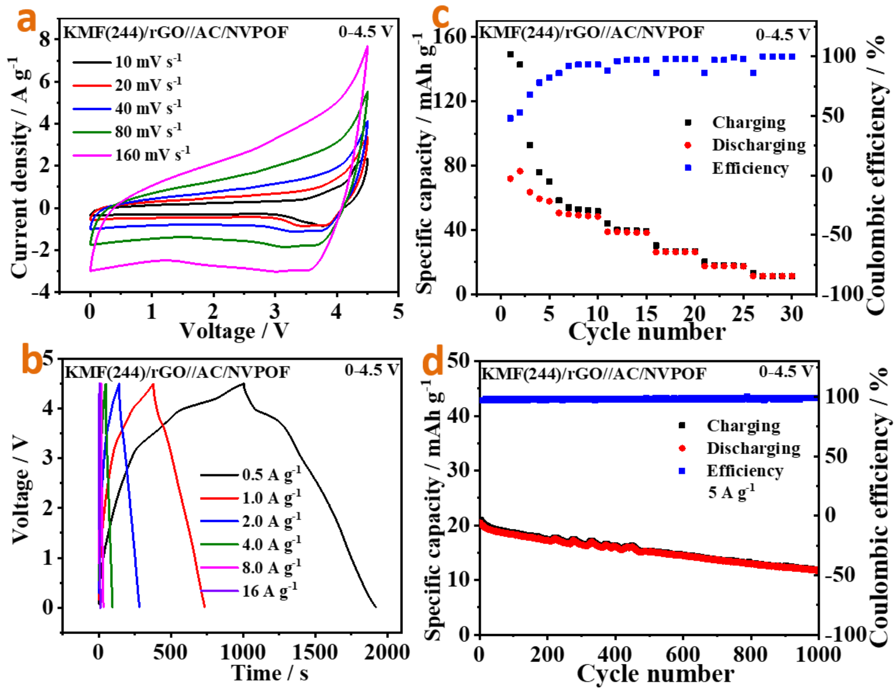

Fig. S19 CV plots at 10-160 mV s^{-1} (a), GCD curves at 0.5-16 A g^{-1} (b), rate capability at 0.5-16 A g^{-1} (c), and cycling behavior at 5 A g^{-1} (d) of the KMF(244)/rGO//AC/NVPOF SICBs under 0-4.5 V.

Table S1 Crystalline parameters for $KNiF_3$, $KCoF_3$, and $KMnF_3$.

Sample	ICSD-PDF	Crystal system	Space group	Cell (a×b×c)/Å^3
$KNiF_3$	21-1002	Cubic	*Pm-3m*	4.0127×4.0127×4.0127
$KCoF_3$	18-1006	Cubic	*Pm-3m*	4.0708×4.0708×4.0708
$KMnF_3$	17-0116	Cubic	*Pm-3m*	4.1890×4.1890×4.1890

Table S2 Charged specific capacity and cycling retention of the KMF/rGO (811-118) electrodes.

KMF/rGO samples	**Specific capacity / mAh g^{-1}**							**Cycle life (500 cycles/0.5 A g^{-1})**
	0.02 (A g^{-1})	0.05 (A g^{-1})	0.1 (A g^{-1})	0.2 (A g^{-1})	0.5 (A g^{-1})	1.0 (A g^{-1})	2.0 (A g^{-1})	
811	228	164	132	105	79	58	42	77%
622	237	166	129	103	75	57	41	65%
424	223	168	131	104	73	54	37	65%
181	138	115	99	85	66	53	41	77%
262	156	124	104	87	68	54	41	72%
442	215	168	132	103	74	56	40	68%
244	**211**	**172**	**147**	**118**	**90**	**71**	**54**	**73%**
226	221	172	137	110	81	60	42	77%
118	136	118	102	86	67	54	41	77%

Table S3 Crystalline parameters for the indicated new phases of the fully discharged/charged state XRD patterns.

Sample	ICSD-PDF	Crystal system	Space group	Cell (a×b×c)/Å^3
Ni	97-064-6091	Cubic	*Fm-3m*	3.5664×3.5664×3.5664
Co	97-005-2934	Cubic	*Fm-3m*	3.5688×3.5688×3.5688
Mn	97-016-3414	Cubic	*P4-32*	6.2747×6.2747×6.2747
KF	01-078-0657	Cubic	*Pm-3m*	3.0600×3.0600×3.0600
NaF	01-071-3747	Cubic	*Fm-3m*	4.6500×4.6500×4.6500
NiF_2	01-071-4806	Tetragonal	$P4_2$-*mnm*	4.6500×4.6500×3.0800
CoF_2	01-070-4977	Tetragonal	$P4_2$-*mnm*	4.6956×4.6956×3.1793
MnF_2	01-083-2419	Tetragonal	$P4_2$-*mnm*	4.8413×4.8413×3.3002
$NaNiF_3$	04-010-7381	Orthorhombic	*Pb-nm*	5.3660×5.5300×7.6950
$NaCoF_3$	01-072-0292	Orthorhombic	*Pn-ma*	5.6070×7.7900×5.4280
$NaMnF_3$	04-002-6582	Orthorhombic	*Pn-ma*	5.6660×7.8280×5.4020

Table S4 Charged specific capacity and cycling retention of the Cathode.

	Specific capacity / mAh g^{-1}							
Current Density / A g^{-1}	0.1 (A g^{-1})	0.2 (A g^{-1})	0.5 (A g^{-1})	1.0 (A g^{-1})	2.0 (A g^{-1})	4.0 (A g^{-1})	8.0 (A g^{-1})	Cycle life (1000 cycles/5 A g^{-1})
AC	74	66	56	48	40	31	22	66%
NVPOF	123	117	105	92	75	53	18	69%
AC/NVPOF	98	90	77	65	50	33	20	60%

Note: The cycling retention was evaluated based on the maximum specific capacity values at the 10th, 20th and 4th cycles for AC, NVPOF and AC/NVPOF electrodes respectively.

Table S5 The design of m_+/m_- ratios for KMF(244)/rGO//AC SICs, KMF(244)/rGO//NVPOF SIBs, and KMF(244)/rGO//AC/NVPOF SICBs.

Systems	**C_m (mAh g^{-1}, 0.1 A g^{-1})**				**m_+/m_-**
	Positive electrode			**Negative electrode**	
	AC	**NVPOF**	**AC/NVPOF**	**KMF(244)/rGO**	
KMF(244)/rGO //AC **(SICs)**	74			147	2.0/1.0
KMF(244)/rGO //NVPOF **(SIBs)**		123		147	1.2/1.0
KMF(244)/rGO //AC/NVPOF **(SICBs)**			98	147	1.5/1.0

Table S6 Performance summary of the KMF(244)/rGO//AC SICs, KMF(244)/rGO//NVPOF SIBs, and KMF(244)/rGO//AC/NVPOF SICBs in this study.

Systems	Working voltage/V	Energy density/ W h kg^{-1}	Power density/ kW kg^{-1}	Cycle life (%/cycles/ A g^{-1})
KMF(244)/rGO//AC **(SICs)**	0-4.5	85.50-74.25 63.00-51.75 36.00-24.75	0.43-0.86 1.69-3.26 6.17-11.14	82%/100/5 A g^{-1} 72%/200/5 A g^{-1} 57%/500/5 A g^{-1} 52%/1000/5 A g^{-1}
KMF(244)/rGO//NVPOF **(SIBs)**	0-4.5	163.97-131.00 91.70-61.70 30.30-17.70	0.66-1.23 2.27-4.19 7.27-13.27	87%/100/5 A g^{-1} 74%/200/5 A g^{-1} 60%/500/5 A g^{-1} 28%/1000/5 A g^{-1}
KMF(244)/rGO//AC/ NVPOF **(SICBs)**	**0-4.5**	**160.00-113.6** **83.76-51.54** **33.00-20.10**	**0.64-1.17** **2.20-4.12** **7.56-15.60**	**90%/100/5 A g^{-1}** **86%/200/5 A g^{-1}** **76%/500/5 A g^{-1}** **60%/1000/5 A g^{-1}**

Table S7 A comparison for the performance of the KMF(244)/rGO//AC/NVPOF SICBs in this study with some reported SICs and SIBs.

	Systems	Voltage window / V	Energy density / W h kg^{-1}	Power density / kW kg^{-1}	Cycle life	Refs.
SIBs	Carbon nanofibers//$NaFePO_4$@C	1.0-4.0	168.1(based cathode active mass)	/	87%/200/0.5 C	[1]
	Se/HMCS//$Na_3V_2(PO_4)_3$/C	1.2-4.2	130	0.052	60%(about)/100/0.5 A g^{-1}	[2]
	FeSe/CNS//$Na_3V_2(PO_4)_3$	0.1-2.7	86(max)	1.58(max)	99.9%/140/1 A g^{-1}	[3]
	PTCDA/NC/CNT// Na_4-PTC/CNT	0.25-3.0	85	0.665	86%(about)/200/0.2 A g^{-1}	[4]
	$Na_3V_2(PO_4)_3$:rGO-CNT// $Na_3V_2(PO_4)_3$:rGO-CNT	1.0-2.2	150	/	77%/100/10 C	[5]
	C//$Na_3V_2(PO)_2F_3$	0.8-4.2	78	/	98.5%/120/0.2 C	[6]
SICs	VN//AC	1.0-4.2	78.43-55.25	0.26-3.9	/	[7]
	$FeVO_4{\cdot}0.6H_2O$//$Na_3(VO)_2(PO_4)_2F$/rGO	0.9-3.1	88-35	0.095-7.9	70%/1000/1 A g^{-1}	[8]
	m-WO_{3-x}@NM-rGO// MSP-20	1.0-4.3	67(max.)	21(max.)	#	[9]
	Ti(O,N)//AC	0.5-4.0	46-10.9	0.046-11.5	82.9%/500/1 A g^{-1}	[10]
	V_2O_5/CNT//AC	0-2.8	38-7.5	0.14-5	80%/900/60 C	[11]
SICBs	**KMF(244)/rGO//AC/NVPOF (SICBs)**	**0-4.5**	**160.00-113.6 83.76-51.54 33.00-20.10**	**0.64-1.17 2.20-4.12 7.56-15.60**	**90%/100/5 A g^{-1} 86%/200/5 A g^{-1} 76%/500/5 A g^{-1} 60%/1000/5 A g^{-1}**	**This work**

Table S8 Chemicals, reagents, and materials used in the study.

Chemicals, Reagents and Materials	Type	Company	Characteristics
$NiCl_2·6H_2O$	AR	SinoPharm	purity≥98.0%
$CoCl_2·6H_2O$	AR	SinoPharm	purity≥99.0%
$MnCl_2·4H_2O$	AR	SinoPharm	purity≥99.0%
$KF·2H_2O$	AR	SinoPharm	purity≥99.0%
PVP-K30	GR	SinoPharm	/
EG	AR	SinoPharm	purity≥99.0%
Graphene oxide (GO)	/	ZhengZhou JingHong New Energy	3-10 floors Conductivity: $2.0*10^5$ S m^{-1} SSA: 150~200 m^2 g^{-1}
Activated carbon (AC)	YEC 8b	FuZhou YiHuan	D50: ~10 μm; Density: 0.4 g cm^{-3}; SSA:2000~2500 m^2 g^{-1}
$Na_3V_2(PO_4)_2O_2F$ (NVPOF)	/	NEWARE	purity≥99.0%
Superconductive carbon black	Battery grade	JH	/
NMP	AR	Kermel	purity≥99.0%
PVDF	Battery grade	JH	/
Electrolytes	Na206-181224	MJS	0.85 M $NaPF_6$ /EC:DEC:EMC (1:1:1) / 5% FEC
Na plate (Homemade)	Battery grade	/	/
Cu foil	200*0.015	GuangZhou JiaYuan	Total thickness: 15 μm; weight: 87 g m^{-2}
Carbon coated-Al foil	222*0.015	GuagZhou NaNuo	Total thickness: 17 μm; Strength: 192 Mpa
Glass microfiber filters	GF/D 2.7 μm; 1823-025	Whatman	Diameter: 25 mm; Thickness: 675 μm; weight: 121 g m^{-2}
Cell components	CR-2032	ShenZhen TianChenHe	/

Table S9 The usage amounts of reagents of the KMF/rGO (811-118) samples.

Samples	Reagent						
	$NiCl_2 \cdot 6H_2O$ (mmol)	$CoCl_2 \cdot 6H_2O$ (mmol)	$MnCl_2 \cdot 4H_2O$ (mmol)	$KF \cdot 2H_2O$ (mmol)	PVP-K30 (g)	GO (g)	EG (ml)
811	1.6	0.2	0.2	5	0.2	0.06	32
622	1.2	0.4	0.4	5	0.2	0.06	32
424	0.8	0.4	0.8	5	0.2	0.06	32
181	0.2	1.6	0.2	5	0.2	0.06	32
262	0.4	1.2	0.4	5	0.2	0.06	32
442	0.8	0.8	0.4	5	0.2	0.06	32
244	**0.4**	**0.8**	**0.8**	**5**	**0.2**	**0.06**	**32**
226	0.4	0.4	1.2	5	0.2	0.06	32
118	0.2	0.2	1.6	5	0.2	0.06	32

References

[1] Y. C. Liu, N. Zhang, F. F. Wang, X. B. Liu, L. F. Jiao, L.-Z. Fan, Approaching the Downsizing Limit of Maricite $NaFePO_4$ toward High-Performance Cathode for Sodium-Ion Batteries, Adv. Funct. Mater. 28 (2018) 1801917.

[2] P. Xue, Y. J. Zhai, N. N. Wang, Y. H. Zhang, Z. X. Lu, Y. L. Liu, Z. C. Bai, B. K. Han, G. F. Zou, S. X. Dou, Selenium@Hollow mesoporous carbon composites for high-rate and long-cycling lithium/sodium-ion batteries, Chem. Eng. J. 392 (2020) 123676.

[3] Z. Xiong, D. D. Sun, X. L. Jia, J. S. Zhou, Core/shell FeSe/carbon nanosheet-assembled microflowers with ultrahigh coulombic-efficiency and rate performance as nonpresodiate anode for sodium-ion battery, Carbon 166 (2020) 339-349.

[4] G. Y. Zhou, L. L. Mo, C. Y. Zhou, Y. Wu, F. L. Lai, Y. Lv, J. M. Ma, Y.-E. Miao, T. X. Liu, Ultra-strong capillarity of bioinspired micro/nanotunnels in organic cathodes enabled high-performance all-organic sodium-ion full batteries, Chem. Eng. J. (2020) 127597.

[5] C. B. Zhu, P. Kopold, P. A. van Aken, J. Maier, Y. Yu, High Power–High Energy Sodium Battery Based on Threefold Interpenetrating Network, Adv. Mater. 28 (2016) 2409-2416.

[6] A. Ponrouch, R. Dedryvère, D. Monti, A. E. Demet, J. M. Ateba Mba, L. Croguennec, C. Masquelier, P. Johansson, M. R. Palacín, Towards high energy density sodium ion batteries through electrolyte optimization, Energy Environ. Sci. 6 (2013) 2361-2369.

[7] S. Q. Wei, C. D. Wang, S. M. Chen, P. J. Zhang, K. F. Zhu, C. Q. Wu, P. Song, W. Wen, L. Song, Dial the Mechanism Switch of VN from Conversion to Intercalation toward Long Cycling Sodium-Ion Battery, Adv. Energy Mater. 10 (2020) 1903712.

[8] J. Dong, Y. He, Y. L. Jiang, S. S. Tan, Q. L. Wei, F. Y. Xiong, Z. L. Chu, Q. Y. An, L. Q. Mai, Intercalation pseudocapacitance of $FeVO_4 \cdot nH_2O$ nanowires anode for high-energy and high-power sodium-ion capacitor, Nano Energy 73 (2020) 104838.

[9] M. S. Kim, E. Lim, S. Kim, C. Jo, J. Chun, J. Lee, General Synthesis of N-Doped Macroporous Graphene-Encapsulated Mesoporous Metal Oxides and Their Application as New Anode Materials for Sodium-Ion Hybrid Supercapacitors, Adv. Funct. Mater. 27 (2017) 1603921.

[10] J. Dong, Y. L. Jiang, Q. D. Li, Q. L. Wei, W. Yang, S. S. Tan, X. Xu, Q. Y. An, L. Q. Mai, Pseudocapacitive titanium oxynitride mesoporous nanowires with iso-oriented nanocrystals for ultrahigh-rate sodium ion hybrid capacitors, J. Mater. Chem. A 5 (2017) 10827-10835.

[11] Z. Chen, V. Augustyn, X. L. Jia, Q. F. Xiao, B. Dunn, Y. F. Lu, High-Performance Sodium-Ion Pseudocapacitors Based on Hierarchically Porous Nanowire Composites, ACS Nano 6 (2012) 4319-4327.